

Article

Not peer-reviewed version

Title Blockiness of 3D Fractured Rocks of Different Fracture Persistence, Spacing, and Orientations

[Maxime Levy Kongandembou](#)*, [Qiyu Wang](#)*, [Yihao Liang](#), [Qingchun Yu](#)*

Posted Date: 30 January 2025

doi: 10.20944/preprints202501.2255.v1

Keywords: fractured rock masses; blockiness; representative elementary volume (REV)



Preprints.org is a free multidisciplinary platform providing preprint service that is dedicated to making early versions of research outputs permanently available and citable. Preprints posted at Preprints.org appear in Web of Science, Crossref, Google Scholar, Scilit, Europe PMC.

Copyright: This open access article is published under a Creative Commons CC BY 4.0 license, which permit the free download, distribution, and reuse, provided that the author and preprint are cited in any reuse.

Article

Title Blockiness of 3D Fractured Rocks of Different Fracture Persistence, Spacing, and Orientations

Maxime Levy Kongandembou ^{1,2,3}, Qiuyu Wang ¹, Yihao Liang ¹ and Qingchun Yu ^{1,*}

¹ School of Water Resources and Environment, China University of Geosciences Beijing, 100083, China

² Laboratoire Hydrosociences Lavoisier, Université de Bangui (Central African Republic)

³ Laboratoire Géosciences, Université de Bangui (Central African Republic)

* Correspondence: yuqch@cugb.edu.cn; Tel.: +8613521206676

Abstract: Understanding the blockiness of 3D fractured rocks with varying fracture persistence, spacing, and orientations is essential for comprehending rock mass behavior, particularly in engineering and geological applications. These factors significantly influence the mechanical behavior, stability, and blockiness of fragmented rock formations. This study aims to analyze the complex behavior of fractured rocks within blockiness fracturing setups using advanced numerical experiments. This study significantly enhances our understanding of how persistence and spacing affect fractured rock formation in three dimensions. Unlike previous studies, our work establishes a fundamental link between fracture geometry and blockiness using parameters of Discrete Fracture Networks (DFNs). Through meticulous analysis and advanced digital experiments, the GeneralBlock software was used to identify and discuss the key components of rupture systems, such as blockiness and representative elemental volume (REV). By establishing DFNs with different parameters, we discovered a fundamental link between fracture geometry and blockiness. The findings indicate that fractured rocks exhibit varied behaviors depending on the blockiness percentage and structural parameters. A higher fracture persistence, lower spacing, and larger angles, limited by the orientation of the fracture surfaces, result in higher L^* values. When L^* was less than 7.36, blockiness was below 1%. When L^* ranges between 7.36 and 22.83, blockiness undergoes a sudden change ranging from 1% to 90%. When L^* exceeds 22.83 and the blockiness surpasses 90%, it gradually stabilizes. These findings are crucial for a better understanding and prediction of the mechanical behavior, stability, and blockiness of fragmented rock formations, with significant implications for engineering and geological applications.

Keywords: fractured rock masses; blockiness; representative elementary volume (REV)

1. Introduction

Rock masses are defined as a collection of blocks of varying dimensions, material discontinuities, stratification surfaces, junctures, and fractures [1]. The impact of persistence, spacing, and occurrence on 3D fractured rock blocks is a complex topic in rock mechanics that significantly affects the behavior and stability of rock masses. Areas known as fractured rock masses initiate, propagate, and merge with macrofractures, leading to the formation of falling rock blocks [2]. Engineers commonly observe this phenomenon, which is attributed to excavation processes [3] and the rearrangement of the geostatic pressure during excavation [4]. The presence of fractured rock masses poses significant challenges in the construction of road infrastructure, tunnel engineering, and drainage channels for water networks, owing to the substantial displacement of the surrounding rock [5]. Understanding fractured rock masses requires assessing the impact of joint persistence and spacing, as these factors form the basis of the continuous-medium method. The analysis of rock block persistence and spacing is fundamental to characterizing fractured rock masses, as the geometry and dimensions of fractures exhibit significant variability. Joint persistence, defined as the extent to which joints propagate within

the rock mass, along with their spatial orientation and spacing, critically influences the block size and configuration of the fractured rock mass. Although it has been known for a long time that joint persistence is a key factor in determining the overall integrity of rock formations, most current rock mass classification systems do not take this into account [6]. Therefore, understanding rock fragmentation relies on the presence of fractures of different sizes within the rock formations.

Numerous indices, some of which are commonly used, such as Rock Quality Designation (RQD) [7], Volumetric Fracture Frequency (J_v), and degree of integrity of the rock mass (K_v) [8], are suitable for quantifying the fracturing extent of a rock mass. Over time, several drawbacks have been highlighted for three frequently utilized indices: (1) impersistent discontinuities are disregarded in the J_v technique, (2) The RQD values are anisotropic, and (3) K_v is subject to other factors [9]. The primary criticism also lies in the fact that these three indices focus solely on discontinuity densities, ignoring the impact of discontinuity persistence, and failing to fully account for the geometric features of discontinuities. According to a study by Kim et al. (2007) [6], discontinuity persistence has an effect that should not be ignored, even if the discontinuity density is the main factor that determines the mechanical characteristics and jointing degree of the rock mass [10]. Xia et al. [11] proposed the concept of blockiness (B), which quantifies and classifies the fracturing extent of a geological formation from the standpoint of block size number in response to the somewhat unsatisfactory nature of the current indices. In addition, the concentration, perseverance, and arrangement of discontinuities are all completely considered and organically integrated into the three-dimensional blockiness concept.

In recent research, the characterization of blocks has been used as an index to categorize the quality of rock masses in recent research. Accurate quantitative analysis of the structural properties of discontinuous surfaces in rock masses is an important challenge for accurately characterizing the structural integrity of rock formations. The fundamental nature of cleavage plays a crucial role in the degree of dispersion of geological formations as they are cut into separate blocks. The fracture persistence, density (spacing), number of groups, number of groups, and orientation of fractures in engineered rock bodies are the main factors influencing the geometric characterization of fractures. In A research study, 77 models were developed for fractured rock formations based on seven fracture-dimension classes and 11 spacing classifications suggested and categorized by the International Society for Rock [12]. The impact of fractures on blockiness is widely acknowledged, particularly about fracture spacing, size, and statistical distribution [13–15]. Rock masses exhibit a wide range of fracture sizes and distributions [11,16]. Fracture spacing and size play pivotal roles in regulating the size, number, and strength of blocks.

This study aims to analyze the identification and composition of rock blocks. Nine iterations were conducted for scope size to minimize the effects of random variations. Additionally, the quantifiable correlation B , fracture interval, and fracture dimension were investigated by assuming equal fracture dimensions, as proposed by Xia and Yu in 2020 [2,11]. The measure of variability was used to indicate the level of dispersion of fracture proportions. Blockiness calculations were performed using the GeneralBlock software, which is capable of analyzing the influence of the fracture geometry parameters on B and REV. The probability of random errors in this relationship was minimized by conducting multiple calculations. This process involved the following steps: 1) Generate the three-dimensional discrete fracture model fracture size, 2) evaluate the blockiness of different fracture formations, and 3) evaluate the effects of persistence, spacing, and orientation on the blockiness of three-dimensional fractures.

2. Generation of Three-Dimensional Discrete Fractures

2.1. Generation of Three-Dimensional Discrete Fractures

2.2.1. Fracture Geometry Parameters

To accurately simulate rock mass structures and faithfully reproduce the natural appearance of field fractures, constructing fracture models that approximate real-world arrangements is crucial for precisely describing the basic elements of fractures, which is a major challenge in the study of rock mechanics. Field observations can capture only the exposed shapes of rock fractures, resulting in limited data availability. Therefore, mathematical methods are typically employed to reconstruct fracture shapes, assuming fracture parameters to be random variables to characterize the stochastic network features of fractures. Describing the developed fracture features within rock masses and constructing three-dimensional spatial models of fractures requires determining parameters such as the spatial position, morphological characteristics, and attribute features of fractures.

Fracture networks can be more accurately represented in numerical models and engineering evaluations using GeneralBlock software. Fracture persistence and spacing are two key factors that affect the size of the geologic formation mass and determine whether it functions as a discrete or an uninterrupted continuum. In contrast, fracture yield affected the shape of the geological formation. Consequently, we focused on the variables of fracture persistence, spacing, and orientation to investigate their effects on fractured rock mass size and REV presence.

To identify rock blocks, representative rock-mass models must be established. By controlling for other variables, the impact of varying the fracture width and spacing on the blockiness of rock formations can be systematically evaluated.

ISRM (1978) [17] classified fracture persistence and spacing into five and seven rates, respectively. The classification of the fracture persistence is listed in Table 1, and the fracture spacing is listed in Table 2. The recommendation provided by the ISRM is considered sufficiently comprehensive to form a foundation for generating various discrete fracture networks (DFNs). The proposed categorization for fracture persistence and spacing can be utilized to model rock masses exhibiting different structural characteristics, ranging from solid to fractured, in a methodological manner.

Table 1. A characterization of fracture persistence constructed on ISRM, 1978.[17].

| Description | Persistence (m) |
|-----------------------------|-----------------|
| Very low persistence (VLP) | <1 |
| Low persistence (LP) | 1-3 |
| Medium persistence (MP) | 3-10 |
| High persistence (HP) | 10-20 |
| Very high persistence (VHP) | >20 |

Table 2. The numerical characterization of the fracture was defined by the ISRM in 1978[17].

| Description | Spacing (mm) |
|-------------------------------|--------------|
| Extremely close spacing (ECS) | <20 |
| Very close spacing (VCS) | 20-60 |
| Close spacing (CS) | 60-200 |
| Moderate spacing (MS) | 200-600 |
| Wide spacing (WS) | 600-2000 |
| Very wide spacing (VWS) | 2000-6000 |
| Extremely wide spacing (EWS) | >6000 |

2.2.2. Fracture Network Modelling

Fractured rock bodies have complex geometric features such as different orientations, lengths, and spacings, and different combinations of these geometric parameters form a complex fracture network within the rock body. Characterizing and analyzing fractured rock masses can be effectively accomplished using fracture network modelling, especially when the DFN approach is applied. It offers insightful information on the behavior, connectivity, and fragmentation of rock masses. Different patterns are present in the cleavage network of rocks, the most common of which are three sets of orthogonal or semi-orthogonal cleavages [20]. In this study, Monte Carlo methods were used to randomly sample fracture persistence, spacing, and orientation based on the fracture disc assumption, using the fracture parameters and the probability density distribution function they obey [21]. Finally, 50 groups of 3D random fracture networks were generated using a computer with the following fracture network parameters (Table 4).

Table 4. Characteristics of 50 anisotropic DFNs: fracture continuity (D in meters), interval (S in meters), and alignment.

| No. | D ₁ | S ₁ | Dip- direction 1 | Dip- angle1 | D ₂ | S ₂ | Dip- direction 2 | Dip- angle2 | D ₃ | S ₃ | Dip- direction 3 | Dip- angle3 |
|-----|----------------|----------------|------------------------|----------------|----------------|----------------|------------------------|----------------|----------------|----------------|------------------------|----------------|
| 1 | 2 | 0.9 | 140.00 | 18.00 | 15 | 0.9 | 144.00 | 69.00 | 15 | 0.04 | 164.00 | 76.00 |
| 2 | 3 | 0.06 | 22.00 | 36.00 | 6.5 | 0.4 | 113.40 | 45.54 | 20 | 1.3 | 243.60 | 80.92 |
| 3 | 65 | 2 | 253.00 | 66 | 3 | 0.4 | 158.00 | 3 | 6.5 | 0.90 | 325.30 | 52.05 |
| 4 | 1 | 0.9 | 219.70 | 4.592 | 6.5 | 0.06 | 125.40 | 48.30 | 2 | 0.9 | 222.00 | 17.64 |
| 5 | 15 | 0.02 | 216.80 | 76.64 | 10 | 0.6 | 19.94 | 56.98 | 10 | 0.2 | 229.60 | 59.78 |
| 6 | 2 | 0.6 | 352.40 | 17.99 | 15 | 0.02 | 171.10 | 76.56 | 1 | 0.04 | 259.90 | 11.21 |
| 7 | 1 | 0.06 | 134.30 | 9.99 | 15 | 2 | 317.70 | 67.56 | 3 | 2 | 204.00 | 28.55 |
| 8 | 20 | 0.2 | 211.30 | 85.55 | 3 | 6 | 258.10 | 26.01 | 3 | 0.9 | 352.70 | 30.57 |
| 9 | 2 | 6 | 33.34 | 12.75 | 15 | 4 | 1.21 | 66.64 | 15 | 0.04 | 42.64 | 75.87 |
| 10 | 10 | 0.02 | 340.50 | 64.36 | 10 | 2 | 128.90 | 54.57 | 15 | 1.3 | 209.30 | 67.93 |
| 11 | 15 | 0.90 | 239.00 | 23.00 | 6.5 | 0.60 | 69.00 | 13.00 | 10 | 0.60 | 264.00 | 2.00 |
| 12 | 1 | 0.6 | 310.90 | 5.55 | 15 | 0.13 | 118.00 | 73.29 | 15 | 0.02 | 208.60 | 77.51 |
| 13 | 2 | 0.4 | 249.00 | 19.14 | 1 | 0.04 | 291.40 | 10.51 | 6.5 | 0.04 | 179.30 | 50.29 |
| 14 | 10 | 0.90 | 221.00 | 2.00 | 3 | 0.60 | 95.00 | 10.00 | 6.5 | 1.30 | 41.00 | 41.00 |
| 15 | 15 | 1.3 | 75.81 | 68.38 | 10 | 0.04 | 91.51 | 62.38 | 6.5 | 0.04 | 295.60 | 49.40 |
| 16 | 1 | 0.4 | 183.10 | 6.72 | 6.5 | 4 | 156.30 | 39.70 | 2 | 0.6 | 281.30 | 18.36 |
| 17 | 10 | 0.04 | 198.30 | 63.29 | 3 | 6 | 288.90 | 26.40 | 6.5 | 4 | 333.10 | 39.70 |
| 18 | 2 | 0.2 | 275.00 | 21.13 | 10 | 6 | 239.90 | 52.53 | 6.5 | 0.06 | 22.91 | 48.42 |
| 19 | 10 | 0.6 | 322.60 | 57.15 | 2 | 4 | 262.00 | 14.56 | 6.5 | 0.4 | 206.50 | 45.83 |
| 20 | 20 | 0.06 | 233.40 | 87.55 | 10 | 0.04 | 43.90 | 63.25 | 20 | 0.4 | 165.40 | 84.07 |
| 21 | 2 | 0.9 | 17.28 | 17.27 | 3 | 0.9 | 102.70 | 30.54 | 2 | 1.3 | 234.60 | 16.21 |
| 22 | 6.5 | 1.30 | 199.00 | 2.00 | 6.5 | 0.60 | 276.00 | 42.00 | 3 | 0.20 | 70.00 | 3.00 |
| 23 | 1 | 0.13 | 256.30 | 8.86 | 10 | 0.9 | 58.92 | 56.83 | 1 | 0.13 | 21.19 | 8.58 |
| 24 | 6.5 | 4 | 110.10 | 39.79 | 20 | 0.4 | 37.35 | 84.68 | 1 | 0.9 | 217.60 | 4.40 |
| 25 | 20 | 1.3 | 153.70 | 81.33 | 3 | 6 | 182.80 | 26.37 | 2 | 0.2 | 225.60 | 20.66 |
| 26 | 15 | 0.9 | 236.20 | 69.92 | 3 | 0.04 | 192.70 | 37.34 | 2 | 0.6 | 47.79 | 18.36 |
| 27 | 10 | 0.6 | 245.50 | 57.10 | 10 | 1.3 | 108.40 | 54.92 | 6.5 | 2 | 98.21 | 41.06 |

| | | | | | | | | | | | | |
|----|-----|------|--------|-------|-----|------|--------|-------|-----|------|--------|-------|
| 28 | 6.5 | 1.3 | 184.90 | 42.40 | 10 | 2 | 299.60 | 54.35 | 10 | 0.6 | 284.20 | 57.70 |
| 29 | 20 | 6 | 242.70 | 77.71 | 15 | 0.06 | 291.70 | 75.34 | 10 | 0.9 | 118.30 | 56.80 |
| 30 | 15 | 6 | 207.90 | 65.54 | 6.5 | 0.02 | 41.41 | 51.43 | 3 | 0.2 | 357.20 | 34.10 |
| 31 | 2 | 1.3 | 135.30 | 16.75 | 15 | 2 | 94.60 | 67.08 | 6.5 | 0.02 | 282.30 | 50.47 |
| 32 | 20 | 0.9 | 62.24 | 82.28 | 2 | 0.13 | 69.15 | 22.08 | 2 | 0.9 | 336.80 | 17.18 |
| 33 | 10 | 1.3 | 239.10 | 54.97 | 10 | 0.02 | 52.74 | 63.50 | 10 | 4 | 224.40 | 53.15 |
| 34 | 3 | 0.6 | 1.22 | 31.94 | 6.5 | 0.6 | 47.95 | 44.95 | 1 | 0.2 | 111.80 | 7.31 |
| 35 | 15 | 2 | 131.50 | 67.34 | 10 | 1.3 | 50.42 | 55.64 | 10 | 0.9 | 156.50 | 56.40 |
| 36 | 10 | 0.04 | 315.80 | 62.83 | 15 | 0.2 | 200.60 | 73.14 | 3 | 2 | 56.25 | 13.56 |
| 37 | 10 | 6 | 347.70 | 52.37 | 20 | 4 | 199.00 | 78.88 | 2 | 1.3 | 283.20 | 82.87 |
| 38 | 10 | 0.9 | 204.20 | 55.88 | 15 | 4 | 300.40 | 66.15 | 15 | 0.02 | 200.30 | 3.93 |
| 39 | 10 | 0.13 | 92.97 | 60.71 | 20 | 0.04 | 258.30 | 88.78 | 3 | 2 | 201.50 | 28.64 |
| 40 | 10 | 6 | 53.05 | 51.75 | 3 | 2 | 91.16 | 27.80 | 2 | 0.13 | 30.95 | 15.81 |
| 41 | 1 | 0.06 | 106.50 | 9.87 | 20 | 4 | 204.80 | 79.00 | 15 | 0.02 | 175.00 | 77.38 |
| 42 | 15 | 2 | 281.70 | 67.67 | 15 | 4 | 190.70 | 14.08 | 3 | 1.3 | 202.90 | 29.72 |
| 43 | 1 | 0.2 | 213.90 | 7.21 | 20 | 0.04 | 247.60 | 6.96 | 10 | 0.4 | 224.50 | 58.27 |
| 44 | 15 | 0.06 | 132.40 | 74.55 | 3 | 2 | 132.60 | 49.55 | 6.5 | 2 | 158.10 | 40.75 |
| 45 | 3 | 0.04 | 52.11 | 37.18 | 20 | 4 | 131.10 | 27.16 | 6.5 | 1.3 | 324.00 | 42.32 |
| 46 | 6.5 | 0.4 | 223.40 | 45.56 | 1 | 0.4 | 134.10 | 13.88 | 3 | 1.3 | 77.74 | 29.37 |
| 47 | 15 | 2 | 91.02 | 67.09 | 6.5 | 0.04 | 96.39 | 28.53 | 15 | 0.06 | 305.00 | 75.15 |
| 48 | 20 | 0.13 | 281.30 | 87.19 | 20 | 4 | 338.50 | 79.40 | 15 | 4 | 89.30 | 65.91 |
| 49 | 3 | 4 | 158.00 | 27.28 | 20 | 0.2 | 190.60 | 85.82 | 1 | 0.02 | 237.00 | 11.57 |
| 50 | 1 | 0.4 | 166.80 | 5.98 | 15 | 04 | 297.90 | 71.36 | 6.5 | 0.13 | 303.00 | 47.69 |

The dimensions of the representative elementary volume (REV) for rock can be appropriately expressed as a multiple of the fracture spacing, typically ranging from two to 20 times this spacing. To ensure that the fracture network's generation range exceeded the study area's size without boundary effects, we defined the fracture network's generation area as a cube with dimensions $L \times L \times L$. This specific relationship can be represented as follows:

$$L = 40S^* + D_{\max} \quad (2)$$

$$S^* = (\Pi S_i)^{1/3} \quad (i=1,2,3) \quad (3)$$

$$D_{\max} = \max(D_1, D_2, D_3) \quad (4)$$

In this context, S^* represents the geometric average of the spacing between the three groups and D_{\max} denotes the highest persistence value observed across these groups. Figure 1 shows the six representative rift models.

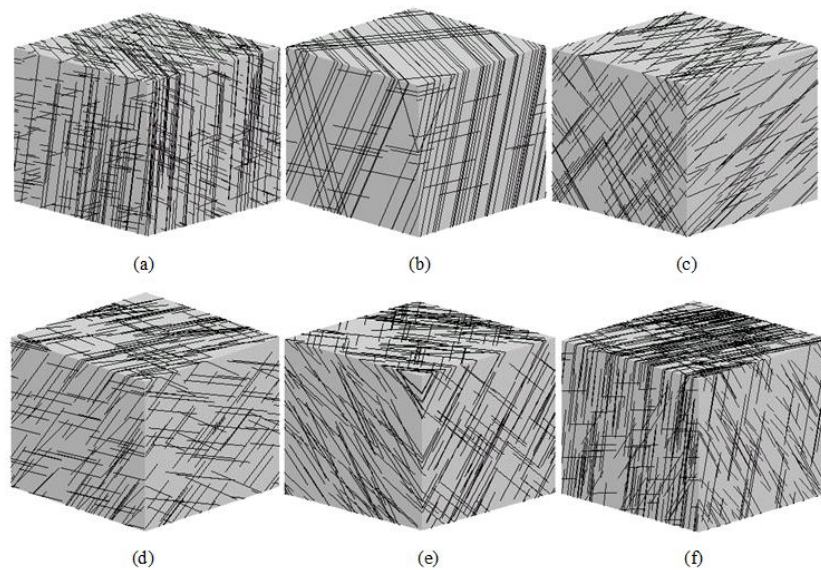


Figure 1. The schematic diagram of six non-orthogonal fracture network models in our 50 discrete fracture networks: (a) F_8 , (b) F_{12} , (c) F_{19} , (d) F_{28} , (e) F_{35} , and (f) F_{37} .

Theoretically, when the range is limited, the blockiness percentage exhibits greater variation. As the range of the model expands, the blockiness percentage tends to stabilize. This was because the three-dimensional fracture density within the simulated rock mass area remained constant. Consequently, a smaller rock mass range encompasses fewer fractures, whereas a larger range incorporates more.

3. Blockiness Analysis and REV Size Estimation of Various Fractured Rocks

3.1. Blockiness of Fractured Rock Mass

Fractures are complexly interconnected within a fragmented rock formation, causing the rock mass to be segmented into multiple, relatively autonomous rock units. The rock mass integrity index provides a quantitative measure of the overall structural stability of a rock formation, which is largely determined by how the fractures within it are interconnected. Specifically, a higher fracture connectivity indicates more extensive fracture development within the rock mass, resulting in greater deterioration of its structural integrity.

The scientific community has developed numerous evaluation systems to measure the deterioration of rock mass integrity owing to fractures. Among these methods, rock quality designation (RQD) has emerged as a widely accepted classic approach. However, these traditional metrics have revealed certain limitations in practical applications, especially the RQD values, and because of their inherent directional sensitivity, it is often difficult to comprehensively capture the subtle fractures that have poor continuity but are numerous in number, and thus may underestimate the actual impact of fractures on rock mass integrity. Three-dimensional discrete fracture network (DFN) modeling has emerged as a popular research area owing to its ability to capture the three-dimensional structural features and integrity of fractured rock masses more accurately. Traditional integrity evaluation metrics, such as RQD, appear to be inadequate because it is difficult to adequately describe and quantify the intricacy and dynamics of the fracture network in a 3D space.

The term “blockiness” refers to the extent to which a rock mass is composed of distinct blocks. This characteristic significantly influences the stability and mechanical properties of rock masses [21]. The blockiness level was determined by assessing the quantity and size of the blocks within the rock mass. A high degree of blockiness suggests extensive jointing in the rock mass, indicating that it should be treated as a discontinuous medium and vice versa. In this context, the block percentage serves as an indicator of blockiness, and is used to quantify the extent of jointing in the rock mass. This percentage was calculated as follows.

$$B = \sum_{i=1}^n V_i / V \times 100\% \quad (5)$$

In this equation, V represents the overall volume of the rock mass and V_i denotes the volume of an individual block i . Variable n indicates the total number of blocks present in the rock mass.

3.2. Estimation of the Blockiness and REV

Effective cleavage, which creates key blocks, can significantly affect the stability of the rock masses. This process can result in various hazards, including rockfalls and landslides. We can forecast potential rock mass stability issues by analyzing the extent of division of a rock mass into separate blocks. Figure 2 illustrates the fractured rock mass model employed to compute different blockiness levels. The range of the model for each rock mass was chosen to be 2–20 times the spacing, demonstrating how the rock mass structure changes when different ranges are selected for the structural model. At the model level, the number of generated fractures ranged from 9 to 523 (Figure 2). The illustration clearly demonstrates that smaller models have fewer crack networks, whereas larger models exhibit an increased number of crack networks.

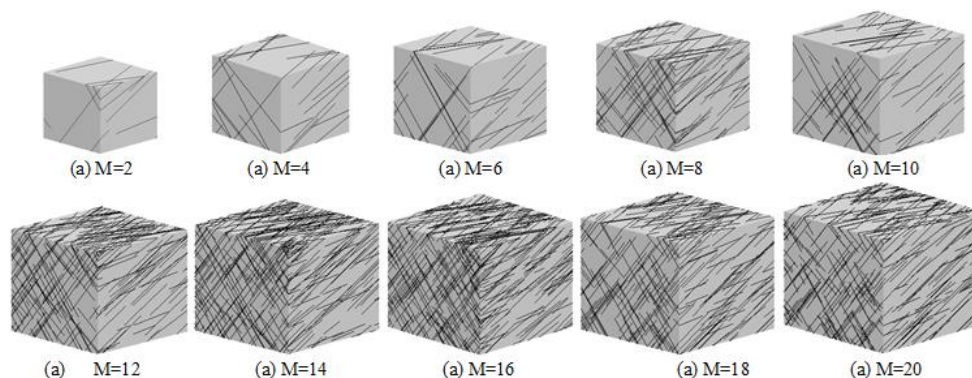


Figure 2. Visualization of rock mass models featuring varying fracture parameter dimensions using a three-dimensional fracture network schematic.

The number of fractures influences the degree of fragmentation in a rock mass, which varies considerably across different geological settings. The model was run several times for each domain size to mitigate the effect of randomness.

The relationship between blockiness and area size is illustrated in Figure 3, which depicts the relationship between B and area size across 12 representative models. The vertical axis represents the blockiness, whereas the horizontal axis shows the domain size. The domain sizes were varied from 2 to 20 times the fracture spacing, with the plotted curve representing the average of nine random iterations.

As illustrated in Figure 3, the principle governing rock mass blockiness follows the same pattern as that controlling porosity, a concept previously explored by Bear. Applying these rock mass models to small volumes often results in significant fluctuations in the blockiness. We identified the REV as the volume at which blockiness stabilized to a constant value. Any noticeable variations in blockiness beyond the REV indicate heterogeneity in the medium. This study assumed that the model cracks were evenly distributed and that blockiness would persist at volumes larger than the REV. In the past, researchers examined how properties change in porous media using both real rocks and numerical models of rocks of different sizes. These studies have examined different properties, rock types, measurement methods, and sample dimensions. Multiple researchers [21–25] have determined that the coefficient of variation (C_v) is an effective measure for quantifying variability across different sample volumes with multiple iterations. A representative effective property was established when C_v fell within the homogeneous range ($0 < C_v < 0.5$) and the corresponding sample volume

approximated the Representative Elementary Volume (REV). Nordahl et al.[26] introduced a method for estimating REV in realistic geological models that explicitly incorporate heterogeneities.

When the fracture spacing increased fourfold, the block percentage in nearly all rock masses underwent substantial change. Nevertheless, rock masses with higher density and extended fracture lengths maintained a consistent block percentage. When the search range was 10, the degree of blockiness in almost all rock masses began to stabilize, aligning with the fracture spacing level.

If the fluctuation range of the block degree was set as the point where it did not exceed 20%, it was considered the stability starting point, and the search range length at this time was designated as the representation unit. Regarding body size, it can be preliminarily assumed that from a swelling degree perspective, most REV fracture rock masses have a size range of 8–18 times the spacing.

The representative elementary volume (REV) for each model was determined as the volume at which the coefficient of variation (C_v) fell below 0.5. Both the measured permeability (both vertically and horizontally) and the correlation lengths of the lithological elements affected the size of the REV. We used the average and variance of blockiness values to assess convergence, whereas C_v quantified the variability across nine random realizations. The blockiness values of the nine realizations required a standard deviation of less than 50% of their mean. The domain size for the calculations can be defined either as mentioned above or as the REV size. The minimum REV was identified as the smallest domain size that satisfied these criteria.

The blockiness and REV for the 50 anisotropic rock mass types listed in Table 4 were computed, and the results are presented in Table 5. The blockiness of each DFN was established when the domain size was 20 times the fracture spacing. We determined the blockiness values for all the 50 anisotropic DFN types. The curve in the figure depicts the average of each calculation outcome. In certain rock mass models, the extent of the rock mass ranges from 8 to 20 times the interfracture spacing.

The degree of blockiness in the fractured rock masses can be assessed using the REV volume, as indicated in Table 5. The analysis revealed that six blockiness values were above 90%, three fell between 80% and 90%, three ranged from 50% to 70%, six were between 10% and 60%, 11 were between 1% and 10%, and the remaining 12 were at 0%. When the blockiness value approaches 100%, it suggests that the rock should be considered a collection of separate blocks. Conversely, a blockiness value near 0% indicates that the rock has good structural integrity.

Table 5. Blockiness percentage table for 50 rock mass models with different DFNs.

| No | B(%) | REV | No | B(%) | REV |
|----|---------|-----|----|---------|-----|
| 1 | 84.1697 | 8 | 26 | 41.6078 | 8 |
| 2 | 5.8664 | 6 | 27 | 0.6968 | 8 |
| 3 | 0.0477 | 8 | 28 | 0.7048 | 10 |
| 4 | 1.1088 | 14 | 29 | 53.6391 | 14 |
| 5 | 95.4269 | 16 | 30 | 8.5866 | 16 |
| 6 | 83.0128 | 8 | 31 | 1.4342 | 12 |
| 7 | 0.2659 | 8 | 32 | 19.7656 | 16 |
| 8 | 0.3314 | 12 | 33 | 4.8809 | 12 |
| 9 | 1.4802 | 16 | 34 | 0.2954 | 12 |
| 10 | 60.8001 | 6 | 35 | 2.3381 | 10 |
| 11 | 0.4089 | 12 | 36 | 91.9793 | 10 |
| 12 | 98.2560 | 14 | 37 | 2.1001 | 10 |
| 13 | 77.8435 | 10 | 38 | 0.2244 | 12 |
| 14 | 0.0008 | 8 | 39 | 97.4617 | 16 |
| 15 | 97.2955 | 12 | 40 | 0.0002 | 8 |

| | | | | | |
|----|---------|----|----|---------|----|
| 16 | 0.0017 | 10 | 41 | 94.1427 | 16 |
| 17 | 0.2988 | 12 | 42 | 0.0019 | 12 |
| 18 | 2.4939 | 10 | 43 | 1.6004 | 8 |
| 19 | 0.8873 | 6 | 44 | 88.3361 | 12 |
| 20 | 89.1926 | 8 | 45 | 0.3696 | 8 |
| 21 | 0.0054 | 6 | 46 | 0.0252 | 12 |
| 22 | 0.0244 | 12 | 47 | 15.1572 | 14 |
| 23 | 4.4814 | 8 | 48 | 6.9122 | 16 |
| 24 | 0.4395 | 8 | 49 | 57.8498 | 16 |
| 25 | 0.0044 | 10 | 50 | 63.3311 | 12 |

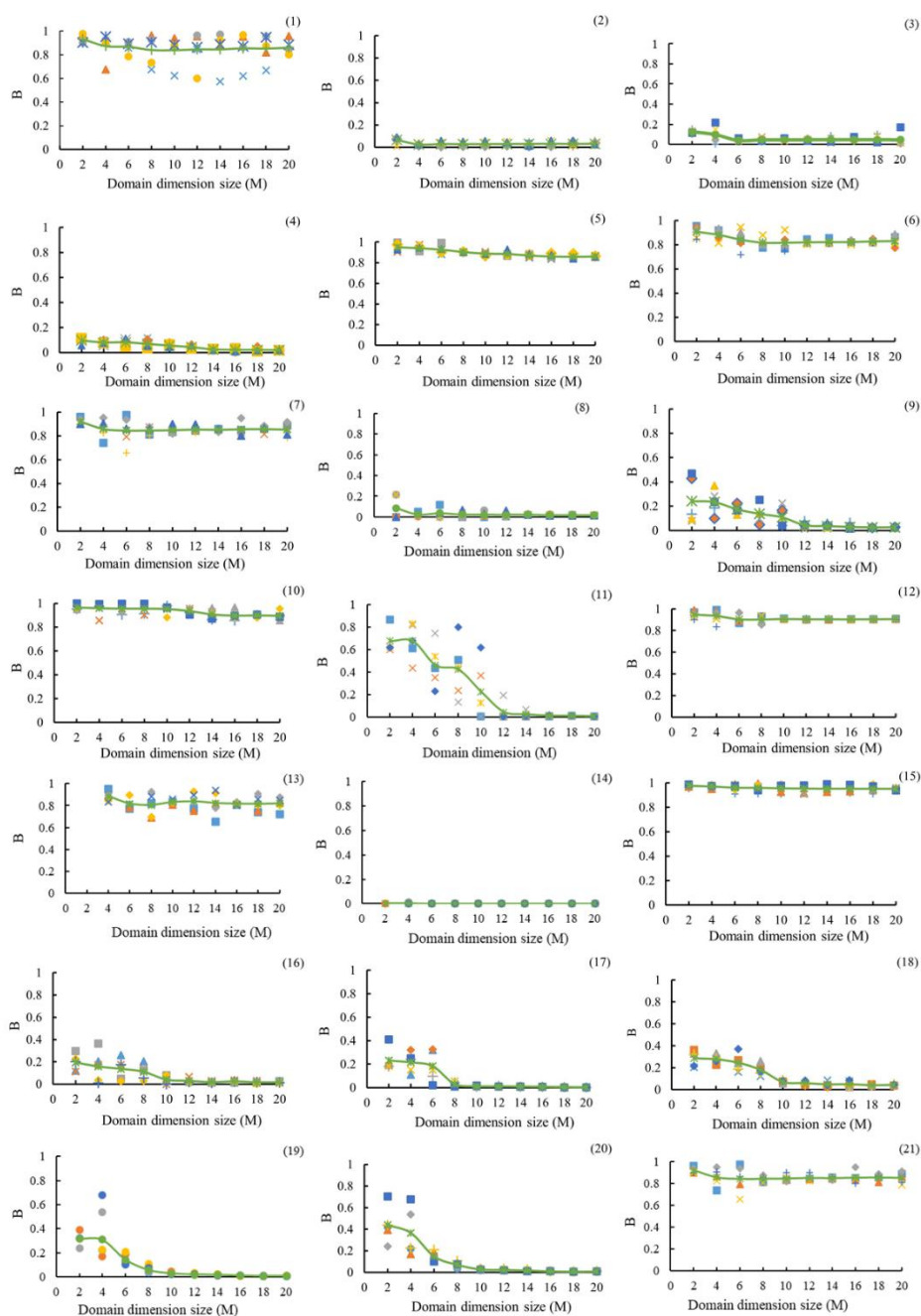


Figure 3. Variation in blockiness between B and domain dimensions in 21 representative models.

We found that angle, distance, and length significantly influence the representative elemental volume (REV) and bulk effects in soils and rocks. Determining the REV and comprehending huge impacts require consideration of the length, angle, and distance. These factors have a direct impact on stability; therefore, they must be carefully considered.

4. Two Types of Fractures That Result in Block Formation

Fracture cutting is a critical process in materials science and engineering and is fundamental for generating a variety of geometric shapes. This study delves into two distinct block shapes that emerge as a result of the fracture cutting. Fracture cutting occurs when a tool or sharp edge penetrates the material, inducing plastic deformation and causing the material to shear along the rake face of the cutting edge [27]. This can result in two primary block formations: radial and shear-type fractures. Radial cleavage fractures originate within the cylinder wall and extend outward to the surface, whereas shear-type fractures occur independently and serve as an energy-dissipation mechanism within the inner portions of the cylinder wall [15]. The formation and propagation of these fractures are strongly influenced by factors such as the wall thickness of the workpiece, the applied loading conditions, and the microstructural properties of the material. Microstructural analysis of the fractured cylinder segments showed a clear connection between the type of fracture and degree of grain boundary distortion. Furthermore, significant shock twinning was noted in the fragments, and the grain structure near the boundary between the fracture surface and untouched material displayed distinctive patterns [28]. The ability of a fracture to produce a block is affected by its length-to-spacing ratio. In rock masses where this ratio is low or where fractures are closely spaced, the random fractures generated by a discrete fracture network model may not fully separate the rock mass into independent blocks. Although some fractures possess a strong cutting capacity, resulting in separate blocks (Figure 4a), others, owing to their spatial arrangement or other constraints, form aggregates of blocks rather than distinct units (Figure 4b). Most natural rock formations exist between the extremes of the continuous media and isolated block systems. Fractured rock masses frequently contain both independent and blocky aggregates. Consequently, this study provides two separate B-value fitting formulas, one for complete cutting and the other for incomplete cutting, and identifies the most suitable fitting approach.

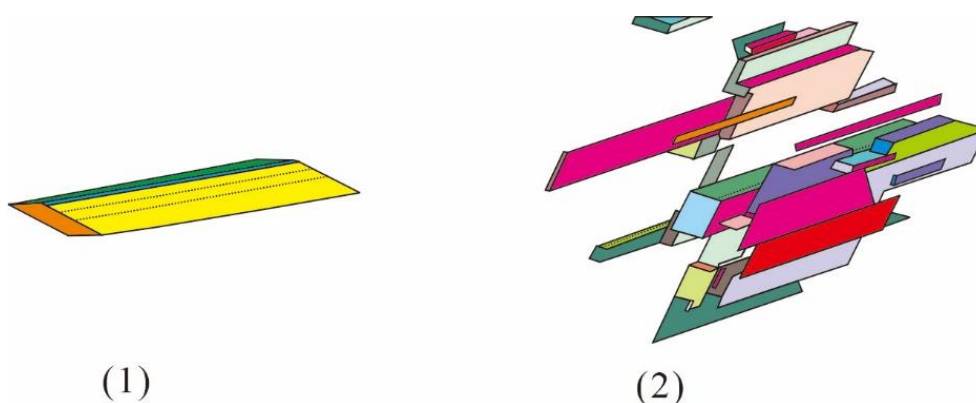


Figure 4. Two block shapes formed by fracture cutting.

5. Effects of Spatial Heterogeneity and Alignment on the Blockiness of 3D Fractures

The anisotropic fractured rock mass is divided into three groups based on ductile spacing and fracture occurrence, which differ. The rock mass is divided into segments by interconnected fractures, and the size and form of these segments are influenced by factors such as fracture tendency, angle of inclination, spacing, and length, as well as a more fragmented rock mass resulting from a higher degree of fracture connectivity. The blockiness effectively gauges the quality and stability of a rock

mass. Overall, blockiness is a key metric for analyzing and classifying fractured rock masses. This is determined by how these variables interact with each other in complex ways.

Solid materials, such as rocks or the Earth's crust, can develop natural fractures due to external pressure. Three groups of principal stresses, represented by fractures 1, 2, and 3, intersect the rock body after it has formed, as shown in Figure 5. Although rocks are typically subjected to three stress-cutting directions, the main stress sets found in nature are not always perpendicular to each other. The accompanying image illustrates how the angles between the primary stresses influence the shape of the rock mass created by intersecting cleavage surfaces. The presence of fractures is a crucial factor for determining whether a rock can be cut into blocks. The size and quantity of the blocks extracted from the fractured rock mass are determined by the fracture persistence and spacing, while the fracture inclination angle dictates whether the resulting rock mass is a cuboid or an oblique prism. Additionally, the relationship between fracture persistence and the length of the intersection between the fracture surfaces can indicate whether the fracture is completely severed.

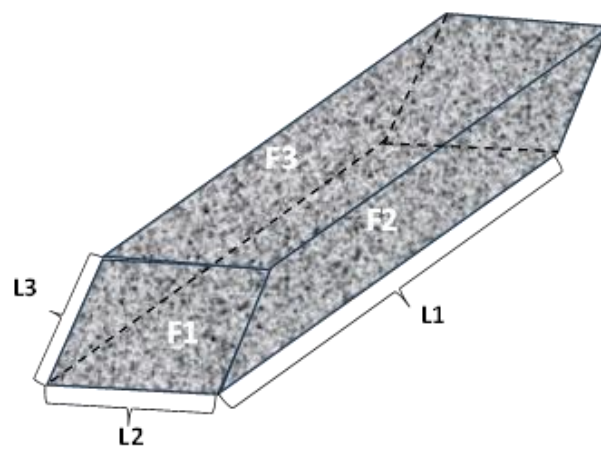


Figure 5. Three-dimensional schematic diagram of the fracture-cut block.

L_3 can also be considered as the length of the edge formed by the cutting of fractures 1 and 2. To visualize and understand the complex three-dimensional geometry of fragmented rock formations, refer to Figure 6. Whether fracture 1 can fully connect the two adjacent fracture surfaces of fracture 3 can be determined by calculating the ratio of the ductility of fracture 1 to L_3 .

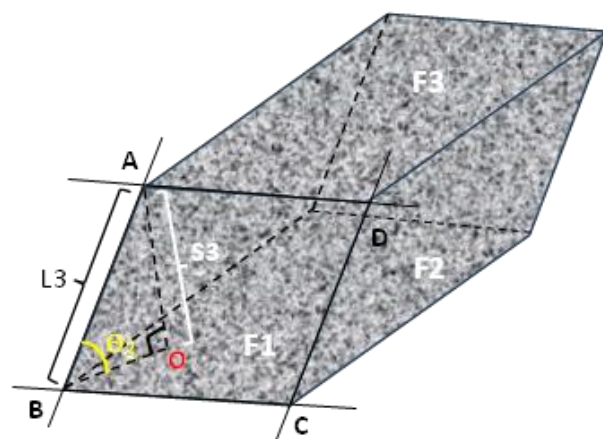


Figure 6. Schematic diagram of the length L_3 (line segment AB) of the intersection line of fracture surfaces 1 and 2 cut by fracture three. (where θ_3 is the angle between the intersection of fracture surfaces 1 and 2 and fracture surface 3).

The lengths L_1 , L_2 , and L_3 of the intersecting lines between fracture surfaces 1, 2, and 3 cut by another fracture were calculated as follows:

$$\begin{aligned} L_1 &= S_1 / \sin \theta_1 \\ L_2 &= S_2 / \sin \theta_2 \\ L_3 &= S_3 / \sin \theta_3 \end{aligned} \quad (6)$$

It was necessary to determine the values of L_1 , L_2 , L_3 , θ_1 , θ_2 , and θ_3 . We consider the normal vectors of fracture surfaces 1, 2, and 3 as n_1 , n_2 , and n_3 , respectively, where $n_1=(a_1,b_1,c_1)$, $n_2=(a_2,b_2,c_2)$, and $n_3=(a_3,b_3,c_3)$. The direction vector of the intersection between fracture surfaces 1 and 2 is denoted as $m_3=(e_3,f_3,g_3)$, whereas the direction vector of the intersection between fracture surfaces 1 and 3 is represented as $m_2=(e_2,f_2,g_2)$. The direction vector of the line formed by the intersection of fracture surfaces 2 and 3 is $m_1=(e_1,f_1,g_1)$. The calculation of m_3 was performed as follows:

$$\vec{m}_3 = \vec{n}_1 \times \vec{n}_2 = (b_1c_2 - c_1b_2, a_1c_2 - c_1a_2, a_1b_2 - b_1a_2) \quad (7)$$

From the above equation, we can introduce the numerical magnitudes of e_3 , f_3 , and g_3 .

$$\begin{aligned} e_3 &= b_1c_2 - c_1b_2 \\ f_3 &= a_1c_2 - c_1a_2 \\ g_3 &= a_1b_2 - b_1a_2 \end{aligned} \quad (8)$$

Similarly, the vector representations of m_2 , m_3 can be obtained, if the normal vector of fracture plane 3 is known to be n_3 , then the angle θ_3 between the intersection line of fracture planes 1 and 2 and fracture plane 3, as well as θ_2 , θ_1 , can be obtained

$$\begin{aligned} \theta_3 &= 90 - \arccos\left(\frac{n_3 \cdot m_3}{|n_3||m_3|}\right) \\ \theta_2 &= 90 - \arccos\left(\frac{n_2 \cdot m_2}{|n_2||m_2|}\right) \\ \theta_1 &= 90 - \arccos\left(\frac{n_1 \cdot m_1}{|n_1||m_1|}\right) \end{aligned} \quad (9)$$

A tetragonal column is formed when the generated fracture completely cuts the rock body. The ratio of different rift persistence values to the shortest distance of complete cutting on the rift surface can be observed in Figure 7 (Equations (10)–(12))

$$L_{12} = D_1 / L_2, L_{21} = D_2 / L_1 \quad (10)$$

$$L_{13} = D_1 / L_3, L_{31} = D_3 / L_1 \quad (11)$$

$$L_{23} = D_2 / L_3, L_{32} = D_3 / L_2 \quad (12)$$

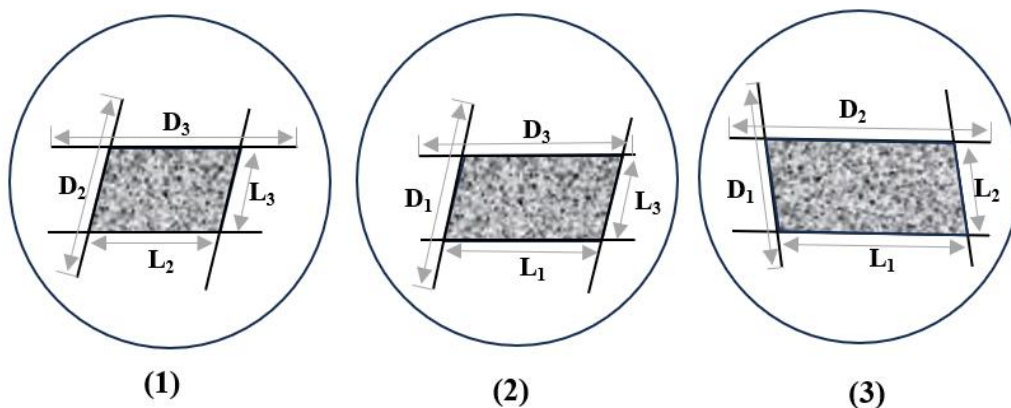


Figure 7. Projection of persistence and spacing onto three sets of fracture surfaces.

The following formula summarizes the six sets of ratios for the three fracture surfaces.

$$L^* = \left(\prod L_{ij} \right)^{1/n} (i=1,2,3; j=1,2,3; i \neq j) \quad (13)$$

The magnitude of the influence of the three factors of ductility, spacing, and yield on the combined influence factor of the level of block mineralization in the case of a fully cut rock body was replaced with the value of L^* .

$$L_{ij} = D_i / L_j (i=1,2,3; j=1,2,3; i \neq j) \quad (14)$$

The relationship between the blockiness, fracture length, and spacing can be represented by an S-shaped surface in geometric terms. In this study, we aim to develop an analytical formula for this relationship using an empirical approach. Drawing from our analysis and discussion, we introduce an S-shaped analytical equation to illustrate how the massing level correlates with the fracture spacing and ductility of the rock mass. This equation is formulated as follows:

$$y = \frac{1}{1 + a(L^*)^{-6}} \quad (15)$$

L^* was fitted to blockiness B to obtain a fitted curve for the blocking level after the rock body was completely cut, as shown in Figure 8.

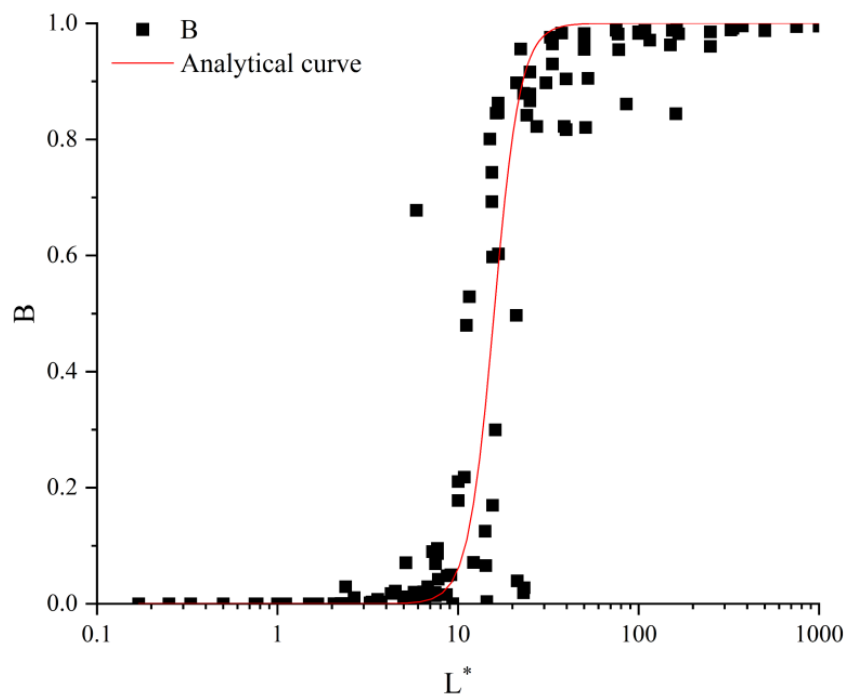


Figure 8. Horizontal adjustment curve blockiness after the complete cutting of the rock formation.

Using the least-squares method, the parameter in Equation 15 was calculated to be $a = 1.57 \times 10^7$, based on the lumped body and L^* values from 50 classes of anisotropic DFNs and 84 classes of isotropic DFNs. A robust relationship was observed between the lumped body and L^* , with a correlation coefficient of $R^2 = 0.83$. Consequently, the following equation was derived:

$$y = \frac{1}{1 + 1.57 \times 10^7 (L^*)^{-6}} \quad (16)$$

When examining the relationship between B and L^* , the rock mass exhibited an S-shaped growth pattern as L^* increased.

Research has shown that the presence of a Representative Elementary Volume (REV) is more likely when persistence and spacing are increased and spacing is more compact. However, most of

these conclusions have been drawn from studies on uniform fractures, neglecting the diversity in spacing and persistence among different fracture sets within the fractured rock mass. The primary factor influencing the effects of persistence and spacing on the REV is the reciprocal cutoff between the spacing of one fracture set and persistence of another. Figure 9 illustrates the relationship between the fracture plane angle and parameters L^* and B.

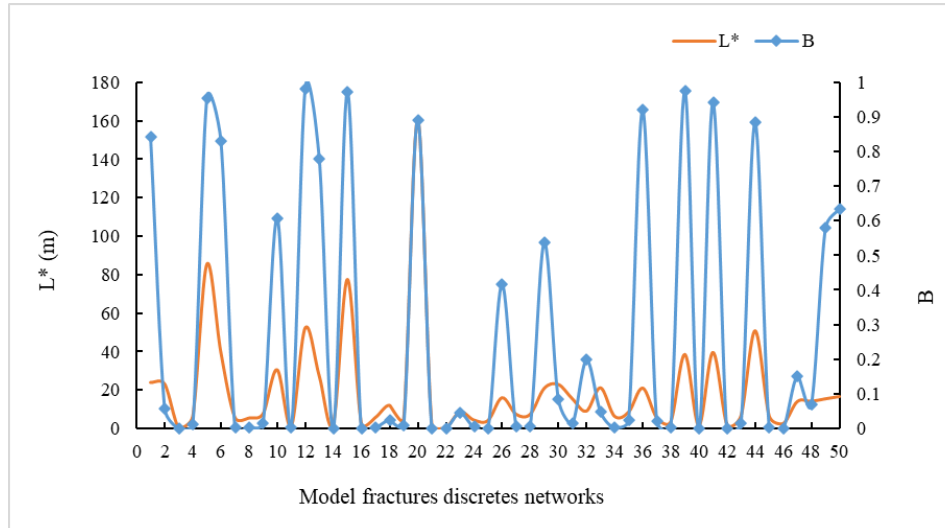


Figure 9. Relationship between L^* and B.

Some cleavages can form blockiness by cutting each other, whereas some cleavages, even if they have a connection, cannot form blockiness through mutual cuts alone. At this point, the main factor is the assembly of blockiness, which is accompanied by the development of independent blockiness. This is why the level of blockiness changes significantly during this period, from 1% to 90%. This is also why the level of massification fluctuates strongly in this interval, and the level of massification fluctuates between 1% and 90%. In the first stage of blockiness development, when $L^* < 7.36$, the fracture cannot cut the rock body to form blockiness or cut blockiness, but cannot be connected to adjacent fractures because of its spatial distribution. L^* causes a gradual increase in the blockiness level and B does not exceed 1%. When it is between 7.36 and 22.83, it enters the second phase of the blockiness mutation. At this stage, the cleavages develop progressively and can form blockiness; however, the spatial distribution of the cleavages has a greater impact. Once L^* surpasses 22.83, the process enters the blockiness stabilization stage. At this point, the impact of the spatial distribution becomes negligible owing to the high cutting capacity of cleavage. The rock mass was predominantly composed of isolated blocks, and B approached 100%. There are two relatively stable phases of blockiness mineralization levels, and there may be some error in discussing the effect of a single factor, ductility, spacing, and yield, on blockiness mineralization levels within these two stable phases. The relationship between the L^* value and blockiness is shown in Figure 9. As the L^* value decreased, the connectivity between the cleavage surfaces and the ability to cut each other to form blocks decreased, and the block size class B also tended to decrease.

6. Conclusions

We used the GeneralBlock program to examine the mechanical properties of a broken rock mass with many joint assemblies that stayed together in different ways. The goal of this study was to determine the mechanical behavior of 3D fractured rock blocks by examining the impact of persistence, spacing, and incidence using statistics. We utilized a statistical experimental design tool to create block systems with varying persistence factors, spacings, and joint orientations. This method was used to create networks that are not orthogonal, speed up simulations, and make it easier to choose the input parameter combinations that define the shape of fractured rock masses.

These findings unequivocally demonstrate that spacing and persistence are the key considerations in the design of engineered rock structures. After looking at 50 different fracture groups in a planned way, I came up with a way to fully look at how ductility, spacing, and incidence affect the presence and appearance of REV. Blockiness influences the overall index L^* . The GeneralBlock software simulations showed that the REV is more likely to occur in cracked rock masses with high L^* values (high ductility, small spacing, and large fracture plane angles) and stable levels of blockiness.

The L^* value is a three-dimensional parameter that can be calculated by comparing the persistence of one set of fractures with the spacing of another set of fractures and the angle between the two fractures. It can be used to measure changes in the REV, history of block-level growth, and types of fractured rock mass blocks. When L^* was less than 7.36, massiveization occurred slowly and did not exceed 1%. This means that few fractures cross to form masses, which supports the strong integrity of the rock mass. For $7.36 < L^* < 22.83$, massing exhibited significant sensitivity to variations in L^* , with the blocking escalating from 1% to 90%. When L^* exceeded 22.83, the body was predominantly segmented into isolated blocks, with blocking values approaching 100%, thereby resembling a collection of discrete blocks.

Three critical criteria substantially affect the dimensions, morphology, and stability of 3D fractured rock blocks, namely orientation, persistence, and spacing. Understanding both their individual and combined effects is important for accurately characterizing rock masses, determining their stability, and designing engineering solutions for a wide range of geotechnical problems. This study conducted a thorough examination of fractured rock masses using these three criteria. Due to the inability to control for variables, individual factors were not analyzed separately. This study did not examine various forms of persistence and gap width distributions, necessitating additional research.

Author Contributions: Conceptualization, K.L.M.; methodology, KLM.; software, K.L.M; validation, KLM., Q.W and Y.L.; formal analysis, K.L.M., and Q.W.; investigation, K.L.M.; resources, Q.Y.; data curation, K.L.M.; writing—original draft preparation, K.L.M.; writing—review and editing, K.L.M.; visualization, KLM., Q.W., and Y.L.; supervision, Q.Y.; project administration, X.X.; funding acquisition, Q.Y. All authors have read and agreed to the published version of the manuscript.

Funding: Not applicable.

Institutional Review Board Statement: Not applicable.

Informed Consent Statement: Not applicable.

Data Availability Statement: All data used to support this study are included in the manuscript

Acknowledgments: In this section, you can acknowledge any support given which is not covered by the author contribution or funding sections. This may include administrative and technical support, or donations in kind (e.g., materials used for experiments).

Conflicts of Interest: The authors declare that they have no known competing financial interests or personal relationships that could have influenced the work reported in this study.

Abbreviations

The following abbreviations are used in this manuscript:

| | |
|----------------|--|
| DFNs | Discrete Fracture Networks |
| REV | Representative elemental volume |
| RQD | Rock quality designation |
| J _v | Volumetric fracture frequency |
| K _v | Degree of integrity of the rock mass |
| ISRM | International society for rock mechanics |

References

- Riquelme, A.J.; Tomás, R.; Abellán, A. Characterization of Rock Slopes through Slope Mass Rating Using 3D Point Clouds. *Int. J. Rock Mech. Min. Sci.* **2016**, *84*, 165–176, doi:10.1016/j.ijrmmms.2015.12.008.
- Chen, S.; Qiao, C.; Ye, Q.; Khan, M.U. Comparative Study on Three-Dimensional Statistical Damage Constitutive Modified Model of Rock Based on Power Function and Weibull Distribution. *Environ. Earth Sci.* **2018**, *77*, 1–8, doi:10.1007/s12665-018-7297-6.
- Feng, X.T.; Guo, H. Sen; Yang, C.X.; Li, S.J. In Situ Observation and Evaluation of Zonal Disintegration Affected by Existing Fractures in Deep Hard Rock Tunneling. *Eng. Geol.* **2018**, *242*, 1–11, doi:10.1016/j.enggeo.2018.05.019.
- Li, G.; Ma, F.; Guo, J.; Zhao, H.; Liu, G. Study on Deformation Failure Mechanism and Support Technology of Deep Soft Rock Roadway. *Eng. Geol.* **2020**, *264*, doi:10.1016/j.enggeo.2019.105262.
- Zhou, H.; Qu, C. kun; Hu, D. wei; Zhang, C. qing; Azhar, M.U.; Shen, Z.; Chen, J. In Situ Monitoring of Tunnel Deformation Evolutions from Auxiliary Tunnel in Deep Mine. *Eng. Geol.* **2017**, *221*, 10–15, doi:10.1016/j.enggeo.2017.02.011.
- Kim, B.H.; Cai, M.; Kaiser, P.K.; Yang, H.S. Estimation of Block Sizes for Rock Masses with Non-Persistent Joints. *Rock Mech. Rock Eng.* **2007**, *40*, 169–192, doi:10.1007/s00603-006-0093-8.
- Singh, B.; Goel, R.K. Rock Quality Designation. *Rock Mass Classif.* **1999**, 17–24, doi:10.1016/b978-008043013-3/50004-3.
- Liu, Q.; Liu, J.; Pan, Y.; Kong, X.; Hong, K. A Case Study of TBM Performance Prediction Using a Chinese Rock Mass Classification System – Hydropower Classification (HC) Method. *Tunn. Undergr. Sp. Technol.* **2017**, *65*, 140–154, doi:10.1016/j.tust.2017.03.002.
- Chen, Q.; Wang, S.; Yin, T.; Niu, W. Improvement of the Concept of the Blockiness Level of Rock Masses. *Arab. J. Geosci.* **2021**, *14*, doi:10.1007/s12517-020-06374-8.
- Barton, N.; Lien, R.; Lunde, J. Engineering Classification of Rock Masses for the Design of Tunnel Support. *Rock Mech. Felsmechanik Mécanique des Roches* **1974**, *6*, 189–236, doi:10.1007/BF01239496.
- Xia, L.; Yu, Q. Numerical Investigations of Blockiness of Fractured Rocks Based on Fracture Spacing and Disc Diameter. *Int. J. Geomech.* **2020**, *20*, 1–10, doi:10.1061/(asce)gm.1943-5622.0001596.
- Elmouttie, M.K.; Poropat, G. V. A Method to Estimate in Situ Block Size Distribution. *Rock Mech. Rock Eng.* **2012**, *45*, 401–407, doi:10.1007/s00603-011-0175-0.
- Ajayi, K.M.; Shahbazi, K.; Tukkaraja, P.; Katzenstein, K. A Discrete Model for Prediction of Radon Flux from Fractured Rocks. *J. Rock Mech. Geotech. Eng.* **2018**, *10*, 879–892, doi:10.1016/j.jrmge.2018.02.009.
- Zhu, H.; Zuo, Y.; Li, X.; Deng, J.; Zhuang, X. Estimation of the Fracture Diameter Distributions Using the Maximum Entropy Principle. *Int. J. Rock Mech. Min. Sci.* **2014**, *72*, 127–137, doi:10.1016/j.ijrmmms.2014.09.006.
- Hu, H.; Xia, B.; Luo, Y.; Gao, Y. Effect of Crack Angle and Length on Mechanical and Ultrasonic Properties for the Single Cracked Sandstone Under Triaxial Stress Loading-Unloading. *Front. Earth Sci.* **2022**, *10*, 1–13, doi:10.3389/feart.2022.900238.
- Yang, Y.; Wang, S.; Zhang, M.; Wu, B. Identification of Key Blocks Considering Finiteness of Discontinuities in Tunnel Engineering. *Front. Earth Sci.* **2022**, *10*, 1–13, doi:10.3389/feart.2022.794936.
- Alber, M.; Yarah, O.; Dahl, F.; Bruland, A.; Käsling, H.; Michalakopoulos, T.N.; Cardu, M.; Hagan, P.; Aydın, H.; Özarslan, A. *ISRM Suggested Method for Determining the Abrasivity of Rock by the CERCHAR Abrasivity Test*; 2013; ISBN 9783319077123.
- Li, A.; Li, Y.; Wu, F.; Shao, G.; Sun, Y. Simulation Method and Application of Three-Dimensional DFN for Rock Mass Based on Monte-Carlo Technique. *Appl. Sci.* **2022**, *12*, doi:10.3390/app122211385.
- Gan, Q.; Elsworth, D. A Continuum Model for Coupled Stress and Fluid Flow in Discrete Fracture Networks. *Geomech. Geophys. Geo-Energy Geo-Resources* **2016**, *2*, 43–61, doi:10.1007/s40948-015-0020-0.
- Zhang, L.; Xia, L.; Yu, Q. Determining the REV for Fracture Rock Mass Based on Seepage Theory. *Geofluids* **2017**, *2017*, doi:10.1155/2017/4129240.
- Kulatilake, P.H.S.W.; Wathugalat, " D N; Stephansson, O. *Joint Network Modelling with a Validation Exercise in Stripa Mine, Sweden*; 1993; Vol. 30;

22. Chen, S.H.; Feng, X.M.; Isam, S. Numerical Estimation of REV and Permeability Tensor for Fractured Rock Masses by Composite Element Method. *Int. J. Numer. Anal. Methods Geomech.* **2008**, *32*, 1459–1477, doi:10.1002/nag.679.
23. Li, Z.W.; Huang, C.Y.; Wang, H.X.; Xing, S.C.; Long, M.C.; Liu, Y. Determination of Heat Transfer Representative Element Volume and Three-Dimensional Thermal Conductivity Tensor of Fractured Rock Masses. *Int. J. Rock Mech. Min. Sci.* **2023**, *170*, doi:10.1016/j.ijrmms.2023.105528.
24. Narendran, V.M.; Cleary, M.P. *ELASTOSTATIC INTERACTION OF MULTIPLE ARBITRARILY SHAPED CRACKS IN PLANE INHOMOGENEOUS REGIONS*; 1984; Vol. 19;.
25. Wang, X.; Zheng, J.; Sun, H. A Method to Identify the Connecting Status of Three-Dimensional Fractured Rock Masses Based on Two-Dimensional Geometric Information. *J. Hydrol.* **2022**, *614*, 128640, doi:10.1016/j.jhydrol.2022.128640.
26. Nordahl, K.; Ringrose, P.S.; Wen, R. *Petrophysical Characterization of a Heterolithic Tidal Reservoir Interval Using a Process-Based Modelling Tool*;
27. Rodríguez, J.M.; Carbonell, J.M.; Jonsén, P. Numerical Methods for the Modelling of Chip Formation. *Arch. Comput. Methods Eng.* **2020**, *27*, 387–412, doi:10.1007/s11831-018-09313-9.
28. Tiedeman, C.R.; Shapiro, A.M.; Hsieh, P.A.; Imbrigiotta, T.E.; Goode, D.J.; Lacombe, P.J.; DeFlaun, M.F.; Drew, S.R.; Johnson, C.D.; Williams, J.H.; et al. Bioremediation in Fractured Rock: 1. Modeling to Inform Design, Monitoring, and Expectations. *Groundwater* **2018**, *56*, 300–316, doi:10.1111/gwat.12585.

Disclaimer/Publisher's Note: The statements, opinions and data contained in all publications are solely those of the individual author(s) and contributor(s) and not of MDPI and/or the editor(s). MDPI and/or the editor(s) disclaim responsibility for any injury to people or property resulting from any ideas, methods, instructions or products referred to in the content.